

Structure in the motions of the fastest halo stars

P. Re Fiorentin^{1,2}, A. Helmi³, M.G. Lattanzi², and A. Spagna²

¹ Dipartimento di Fisica Generale, Via Pietro Giuria 1, 10125 Torino, Italy.

² INAF - Osservatorio Astronomico di Torino, Strada dell'Osservatorio 20, 10025 Pino Torinese, Italy.

³ Kapteyn Astronomical Institute, P.O. BOX 800, 9700 AV Groningen, The Netherlands.

Received, 2005; accepted, 2005

Abstract. We have analyzed the catalog of 2106 non-kinematically selected metal poor stars in the solar neighborhood published by Beers et al. (2000), with the goal of quantifying the amount of substructure in the motions of the fastest halo stars. We have computed the two-point velocity correlation function for a subsample of halo stars within 1 – 2 kpc of the Sun, and found statistical evidence of substructure, with a similar amplitude to that predicted by high resolution CDM simulations. The signal is due to a small kinematic group whose dynamical properties are compared to the stellar "stream", previously discovered by Helmi et al. (1999). If real, this high velocity moving group would provide further support to the idea that substructures remain as fossils from the formation of the Galaxy as expected in the CDM scenario.

Key words. Galaxy: formation – Galaxy:halo – Galaxy:kinematics

1. Introduction

Observations of metal-poor stars have many times been used to discriminate (although not yet conclusively) between alternative galaxy formation scenarios (e. g., Eggen, Lynden-Bell & Sandage 1962; Searle & Zinn 1978). In recent years, considerable effort has been put into understanding the properties of galaxies within the hierarchical paradigm of structure formation in the Universe which, so far, looks to be the most successful theory. In a CDM Universe, the first objects to form are small galaxies which then merge and give rise to the larger scale structures we observe today. Thus, structure formation occurs in a 'bottom up' fashion. This theory predicts the presence of substructures (tidal tails, streams) due to the mergers and accretion that galaxies have experienced over their lifetime.

Direct comparisons to observations have shown that this model can reproduce the properties of both the local and the distant Universe. Several examples of mergers and galaxy interactions have been observed in the Milky Way, such as the disrupted Sagittarius and Canis Major dwarf galaxies (e. g., Ibata et al. 1995; Martin et al. 2004), the phase-space stream of halo stars in the solar neighborhood (Helmi et al. 1999), and the ring in the outer Galaxy (Newberg et al. 2002). Similar substructures have also been found in the halos of other nearby galaxies, such as M31 (Ferguson et al. 2002) and NGC 5907 (Zheng et al. 1999), showing that accretion may be a common phenomenon in the evolution of galaxies.

Although the stellar halo accounts for only about 1% of the luminous mass, it plays a crucial role in studies of formation and evolution of the Galaxy. Signatures of the hierarchical nature of galaxy assembly are expected to be most obvious in this component. Moreover, stars in the halo are generally very old and metal poor, i.e. they can be considered more pristine. These are in fact the stars thought to have been formed in satellite galaxies that merged to form our Galactic halo (Robertson et al. 2005).

At present, the best measurements of the halo kinematics are obtained from the analysis of samples of stars located in the solar neighborhood. Studies of the kinematics of various stellar populations in the Galaxy have long been limited - especially for the inner Halo - by the lack of large samples of stars with accurate distances, metallicity and kinematics.

Beers et al. (2000) compiled an extensive catalog of metal-poor stars selected without kinematic bias, and with available proper motions, radial velocities, and distance estimates for stars with a wide range of metal abundances. In this paper we analyze this data-set, which has already provided support for constraining plausible scenarios for the formation and evolution of the Milky Way (e. g., Chiba & Beers 2000, 2001).

The layout of this paper is as follows: In Sect. 2, we assemble a sample of metal-deficient ($[Fe/H] \leq -1.5$ dex) halo stars up to 2 kpc of the Sun selected from the Beers et al. (2000) catalog. In Sect. 3, we explore their phase-space distribution and quantify clustering by means of the two-point correlation analysis. In Sect. 4, we compare to theoretical predictions from CDM simulations. In Sect. 5, we further examine evidence for kinematic substructure in the space of adiabatic invariants. The conclusions of the present study are given in Sect. 6.

2. Halo samples from Beers et al. (2000) catalog

Beers et al. (2000) presented a revised large catalog of 2106 metal poor stars in the solar neighborhood selected without kinematic bias. Within this sample, 1258 stars have distance estimates and radial velocities as well as proper motions, so that the three components of the space velocities can be derived.

Throughout this work we adopt Galactic velocity components relative to the Galactic center, where as usual U , V and W are positive toward the center, in the direction of the rotation, and toward the north Galactic pole, respectively. We assume that the local standard of rest (LSR) rotates with a velocity of 220 km s^{-1} about the Galactic center, and that the peculiar velocity of the Sun relative to the LSR is given by $(10.00, 5.25, 7.17) \text{ km s}^{-1}$ (Dehnen & Binney 1998).

2.1. Selection criteria and selected sets

Since we are interested in constructing a sample of halo stars, we will only consider those stars in the Beers et al. (2000) catalog with metallicities $[\text{Fe}/\text{H}] \leq -1.5$ dex.

To minimize any possible contamination from the thick disk, we further exclude low metallicity stars near the plane and with coplanar and circular orbits, i.e. with disk-like kinematics. Assuming an exponential thick disk with scale height $0.8 \text{ kpc} < h_z < 1.5 \text{ kpc}$ (Reid & Majewski 1993; Robin et al. 1996) and with a velocity ellipsoid $(\sigma_R, \sigma_\phi, \sigma_z; \langle V_\phi \rangle) = (61, 58, 39; -36) \text{ km s}^{-1}$ (Binney & Merrifield 1998), we exclude those stars for which the following conditions are *simultaneously* satisfied: $|Z| \leq 1.5 \text{ kpc}$, $126 \text{ km s}^{-1} \leq V_\phi \leq 242 \text{ km s}^{-1}$, $|V_R| \leq 61 \text{ km s}^{-1}$, low angular momentum $L_{xy} = \sqrt{L_x^2 + L_y^2}$ with respect to L_z , namely $|L| \leq 1.1 L_z$.

Table 1. Selected sets of metal deficient ($[\text{Fe}/\text{H}] \leq -1.5$ dex) halo stars. See text for explanation.

Type		1 kpc	2 kpc
D	main-sequence dwarf star	11	13
A	main-sequence A-type star	2	3
TO	main-sequence turnoff star	73	169
SG	subgiant star	1	9
G	giant star	78	133
AGB	asymptotic giant branch star	5	5
FHB	field horizontal-branch star	5	5
RRV	RR Lyrae variables	16	70
V	variable star	1	3
TOTAL		192	410

The remaining stars define our *selected* sample. This sample contains 192 stars within 1 kpc and 410 within 2 kpc of the Sun. These sets include subdwarfs, giants, and variables, as described in Table 1, with the following properties:

- proper motions are available from the HIPPARCOS Catalog for 197 stars; the other ground-based measurements come from the SPM Catalog 2.0, Lick NPM1 Catalog, STARNET Catalog, ACT Reference Catalog; for stars independently measured in two or more catalogs, we have averaged the proper motions weighted by their errors; in all cases accuracies of a few mas yr^{-1} are achieved.
- Radial velocities have typical accuracies of the order of 10 km s^{-1} . Metal abundances have been determined either spectroscopically or from suitable photometric calibrations.
- Calibrations of absolute magnitude M_V allow photometric parallaxes for which Beers et al. (2000) claim an accuracy of $\sim 20\%$. Because of the large distance ($d > 200 \text{ pc}$), these photometric parallaxes are, formally, more precise than the corresponding HIPPARCOS trigonometric parallaxes, however they still remain the main source of uncertainty in the derived tangential velocities.

3. Kinematic analysis

Analytic arguments and high-resolution cosmological simulations of the formation of dark matter halos (Helmi & White 1999; Helmi et al. 2002; Moore et al. 2001) suggest that the halo should be spatially smooth in the Solar neighborhood (although see some recent discussion in Diemand et al. 2005; and Zhao et al. 2005). This is also supported by measurements of the degree of lumpiness in the angular distribution of halo stars (e.g. Lemon et al. 2004). However, the same simulations predict that while the kinematics of halo objects near the Sun can be represented by a smooth multivariate Gaussian distribution, the motions of the most energetic particles should be strongly clumped and anisotropic. This result has motivated us to analyze in more detail the kinematics of the halo samples we identified above.

3.1. Velocity distribution

The motion of each star in the sample can be specified by the velocity vector $\mathbf{v} = (U, V, W)$ in 3D linear space, as well as in the 2D angular space, by spherical angular coordinates $\alpha = (\phi, \theta)$, where $\sin \theta = V_z/|\mathbf{v}|$ and $\tan \phi = V_y/V_x$.

Figure 1 shows the kinematic distribution of the selected sample within 1 kpc. In Fig. 1(a-c) we plot the U, V, W velocities. Fig. 1(d) shows the distribution of velocity directions $\alpha = (\phi, \theta)$.

The velocity distribution is relatively smooth, and appears to be consistent with a Gaussian Schwarzschild distribution. The mean velocities are $(\langle U \rangle, \langle V+220 \rangle, \langle W \rangle) = (-26 \pm 11, 21 \pm 8, -1 \pm 7) \text{ km s}^{-1}$ and the velocity ellipsoid is radially elongated, namely $(\sigma_U, \sigma_V, \sigma_W) = (150 \pm 8, 106 \pm 5, 96 \pm 5) \text{ km s}^{-1}$. However, a smooth description does not seem to reproduce the kinematics of the the fastest objects, as shown by the highlighted points. The 5% fastest moving stars (light color dots) seem to be more clumped. The characteristics of the observed velocity distribution appear to be in rough agreement with the results of CDM simulations as we shall show in Sect.5.

We shall perform two different statistical tests on the data with the aim of quantifying the presence of large and small

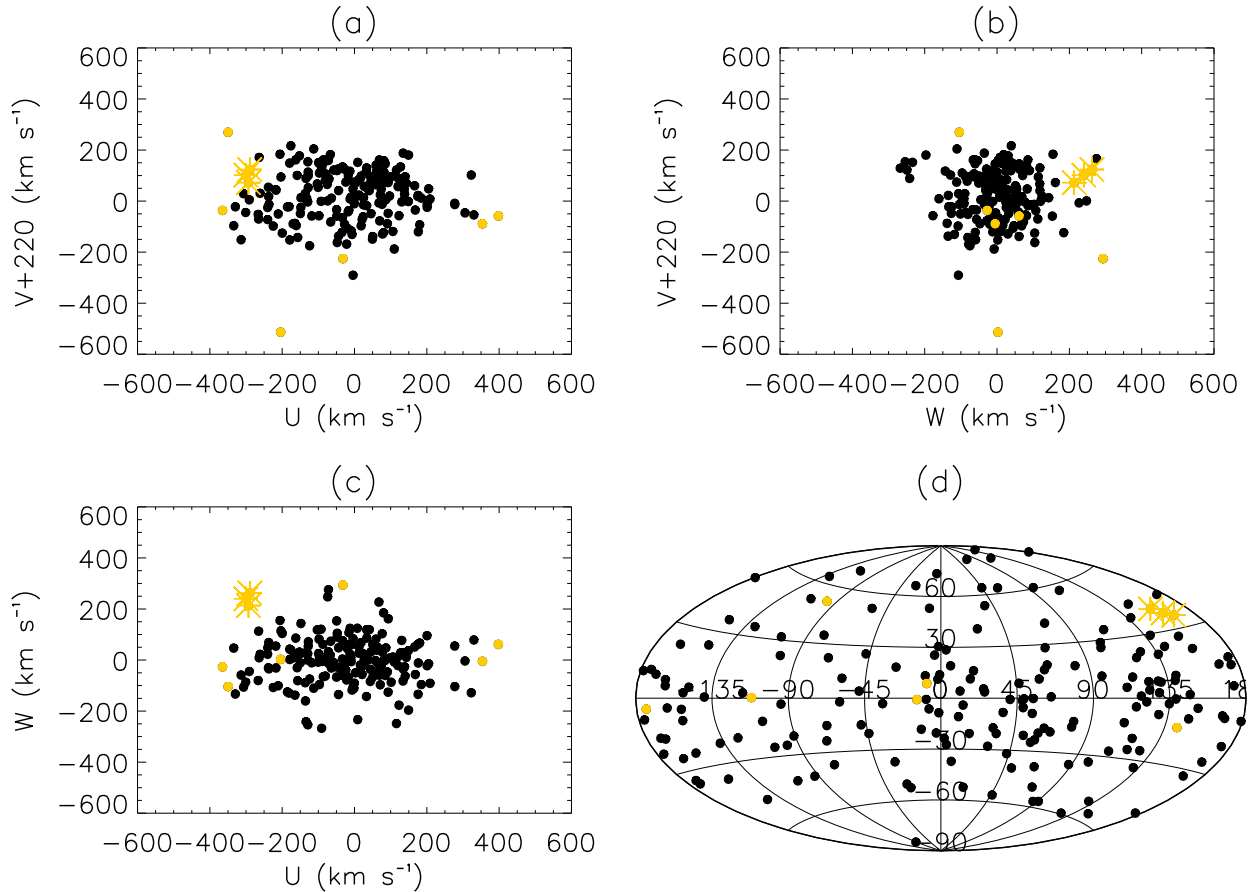


Fig. 1. Distribution of nearby halo stars in velocity space for our selected sample with $[\text{Fe}/\text{H}] \leq -1.5$ dex within 1 kpc of the Sun. (a-c) Velocity projections in the (U, V, W) space; (d) Velocity direction: the position of each particle is given by the spherical angular coordinates $\alpha = (\phi, \theta)$ of the velocity vector. Of the 192 stars present in this volume, the 5% fastest are highlighted as light color dots. Among them, the asterisks identify the objects/groups with velocity difference less than 42 km s^{-1} .

scale anisotropies in the motions of our stars. To establish the significance of our results we will compare our results to suitable Monte Carlo simulations.

Our synthetic data sets have the same number of stars and the same spatial distribution as the observed sample. The characteristic parameters of the multivariate Gaussian used to describe the kinematics are obtained by fitting to the observed mean values and variances after appropriate convolution with observational errors. We generate 100 ‘observed’ samples as follows. A velocity is drawn from the underlying multivariate Gaussian; it is transformed to a proper motion and radial velocity (assuming the observed parallax and position on the sky); observational ‘errors’ of the magnitude described in Sect.2 are added to the parallax, the radial velocity and the proper motion; these ‘observed’ quantities are then transformed back to an ‘observed’ velocity.

The first test we perform on the data consists in quantifying the presence of large-scale anisotropies. We implement this test by partitioning the 2D angular space (ϕ, θ) -see Fig. 1(d)- into cells with roughly similar area. We then count how many stars fall in each cell and compare it to the expected number in our Monte Carlo simulations.

Figure 2 shows the results for the partition with 24 cells (with an area of $1800 - 1500 \text{ deg}^2$) along 4 strips: $0^\circ < |\theta| < 45^\circ$ (with $\Delta\phi = 45^\circ$) and $45^\circ < |\theta| < 90^\circ$ (with $\Delta\phi = 90^\circ$). Plotted are the counts in each cell for the selected halo sample within 1 kpc of the Sun (solid line) and for the average of 100 Monte Carlo realizations (dashed line). The east-west large-scale anisotropy seen in this figure is due to the radially elongated velocity ellipsoid in combination with a small amount of prograde rotation.

We find, at the 1σ level, an excess of stars due to residual contamination from the thick-disk ($\phi \sim 90^\circ$) and a lack of stars moving toward the SGP ($\theta \sim -90^\circ$). To this regard, it is interesting to note that this deficiency is at odds with some models of the Sagittarius dwarf evolution that predict the presence of a stellar stream that should cross the Solar neighborhood. The stream would be visible as an excess of stars moving toward the SGP (e.g. Helmi 2004a; Law et al. 2005). Even though it could be argued that this sample may be too bright and possibly too metal-poor, this result could rule out an oblate or spherical shape for the Galactic dark-matter halo, and favor a prolate mass distribution as suggested by Helmi (2004b).

In summary, the observed and simulated counts are statistically indistinguishable for all partition choices. There is no ev-

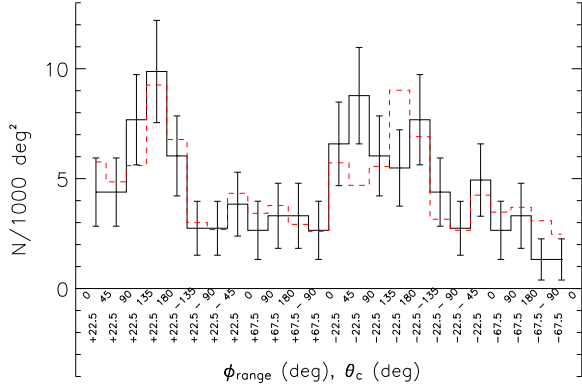


Fig. 2. (ϕ, θ) -space number counts for a partition with 24 cells with $\Delta\theta = 45^\circ$ (mean value θ_c) and $\Delta\phi = 45^\circ/90^\circ$ for the stripes along the equator and close the poles respectively. The solid line corresponds to the selected sample within 1 kpc of the Sun, while the dashed histogram to the average number of counts in our Monte Carlo simulations. Error bars are based on Poisson statistics.

idence (at $> 2\sigma$ -level) for large scale flows crossing the Solar neighborhood.

3.2. Correlation function

We quantify the deviations from a smooth Gaussian distribution due to kinematic substructures by means of the two-point correlation function, defined as

$$\xi = \frac{\langle DD \rangle}{\langle RR \rangle} - 1 \quad (1)$$

where $\langle DD \rangle$ is the number of pairs of stars in our data with velocity difference less than a given value, namely

$$\langle DD \rangle = \sum \text{pairs of stars } i, j \text{ with } |\mathbf{v}_i - \mathbf{v}_j| \leq \Delta \quad (2)$$

and $\langle RR \rangle$ is defined analogously for the same number of random points drawn from a multivariate Gaussian distribution derived from the data set, convolved with expected observational errors, and averaged over a hundred realizations. Note that the points are not statistically independent, and that our definition of ξ actually corresponds to the cumulative correlation function often used in cosmology in studies of the large-scale structure of the Universe (e.g., Coil et al. 2004; Mullis et al. 2004).

Based on Poisson counts, we estimate the error of the two-point correlation function as

$$\Delta_\xi = \frac{1 + \xi}{\sqrt{\langle DD \rangle}} \quad (3)$$

Thus, in the 3D linear space (U, V, W) - say $v = |\mathbf{v}_i - \mathbf{v}_j|$ - $\xi(v)$ measures the excess of pairs of stars moving with velocity difference equal or smaller than a given value, above that expected from a random sample. Clumping due to kinematic

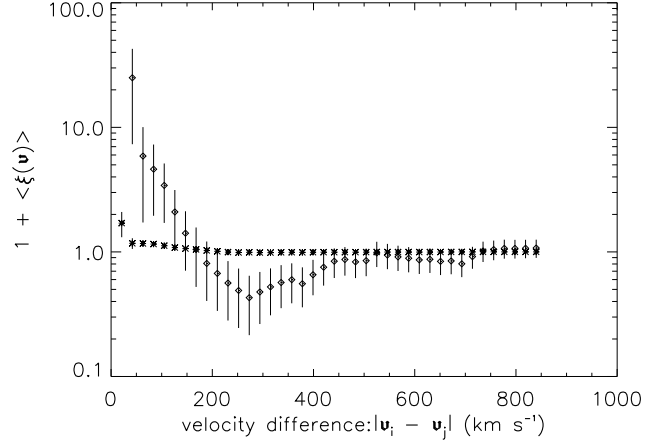


Fig. 3. Two-point velocity correlation function for our selected sample within 1 kpc (asterisks) and for the 5% fastest moving stars (diamonds). In both cases, there is a signal at small velocity differences, indicative of the presence of streams. The error bars are based on Poisson counts.

substructures (i.e. groups of stars moving with similar velocities) is manifested by an excess at small velocity separations.

In Figure 3 we show the two-point correlation function $\xi(v)$ for our selected sample within 1 kpc of the Sun (asterisks) and a subset comprising the 5% fastest-moving stars (diamonds). We use bins of width 21 km s^{-1} , up to separations of 840 km s^{-1} .

The figure shows that, at a 1σ level, there is a small but statistically significant excess of stars with similar velocities with respect to what would be expected for a smooth Gaussian distribution. The signal in the first bin is weak but significant. No correlation is observed at larger separations.

However the signal is clearly much stronger for the subset of 5% fastest moving stars: in this case, the excess of pairs of stars with similar velocities is very noticeable, and it is a direct indication of the presence of clumps/streams. This signal is indeed due to a moving group, which is formed by three stars (described in Table 2) and indicated by the asterisks in Fig. 1.

Note also the presence of a certain degree of anti-correlation for the interval $200 - 400 \text{ km s}^{-1}$. This may be due to a type of ‘clear out effect’ as the result of the clumping of few objects within the first bins. This effect would have a considerably smaller amplitude for a larger sample (as is the case when our selected sample is considered in its entirety).

So far we have focused on the 5% fastest moving particles within 1 kpc of the Sun. Analysis performed with the 10% fastest subsample still shows a significant deviation from a multivariate Gaussian, albeit of smaller amplitude.

Turning to an eight times larger volume (we consider those stars within 2 kpc of the Sun) allows us to increase the number of stars, but only by a factor of ~ 2 . This increase in the number of stars, does not necessarily translate into an enlargement of the number of streams but could also lead to a better representation of each stream.

However this effect is not obvious in our sample: for the larger volume the kinematic group previously singled out loses

Table 2. Members of the identified moving group.

Name	[Fe/H] (dex)	α (J2000) (h m s)	δ (J2000) (d m s)	D (kpc)	U (km s ⁻¹)	$V + 220$ (km s ⁻¹)	W (km s ⁻¹)
BPS CS 30339 – 0037	-2.13	00 20 28.90	-36 12 00.7	0.80 ± 0.16	-292 ± 54	73 ± 36	214 ± 12
HD 214161	-2.16	22 37 08.04	-40 30 38.4	0.62 ± 0.12	-290 ± 23	123 ± 22	262 ± 15
V* RZ Cep	-1.77	22 39 13.05	+64 51 28.9	0.41 ± 0.08	-301 ± 62	101 ± 27	240 ± 47

one star, BPS CS 30339-0037, which is no longer selected in the 5% high velocity tail (simply a consequence of small number statistics). Up to velocity difference smaller than 42 km s^{-1} , a weak signal (at the 1σ level) is noticeable: it is due to the two remaining stars of our moving group and a second structure with two other stars. Given the low amplitude of this signal in comparison to the 1 kpc sample, we are led to believe that this second structure is probably a statistical fluke rather than a true physical system.

In summary, we have detected a moving group (with three members) among the 5% most energetic stars within 1 kpc of the Sun; no other members could be found by increasing the volume or relaxing the velocity threshold (from 5 to 10%).

4. Comparison to the Theory: Simulations

We now wish to compare our results from the previous section to theoretical models. To this end, we use a high-resolution simulation of the formation of a dark matter halo in a Λ CDM cosmology (Springel et al. 2001). From this simulation, we derive the kinematics of dark matter particles inside spheres of 2 kpc radius, located at 8 kpc from the Galactic center. In doing so, we are assuming that these volumes are representative of the solar neighborhood.

In Fig. 4 we plot the kinematics of 2348 particles selected within one of the 2 kpc spheres. Their velocity distribution is relatively smooth and appears to be quite consistent with a multivariate Gaussian (see Fig. 5), with principal axes $(\sigma_1, \sigma_2, \sigma_3) = (143, 118, 110) \text{ km s}^{-1}$. However, if we focus on the motions of the most energetic particles (indicated with gray symbols in Fig. 4) this is no longer the case. The 5% fastest moving particles are strongly clumped, and their distribution is highly anisotropic.

To quantify the substructures present in this volume we compute the velocity correlation function ξ (as described in Sect. 3). The random comparison sample in this case is the result of averaging 100 realizations of a trivariate Gaussian with similar moments as the dark matter velocity distribution. In Fig. 5 we observe a weak signal in the first bins produced by a small excess of particles with similar velocities (asterisks). However, if we focus on the 5% fastest moving particles (diamonds), the excess has a much larger amplitude particularly at small velocity differences (i.e. $\Delta v < 42 \text{ km s}^{-1}$), and simply reflects the presence of kinematic groups clearly visible in Fig. 4.

Although the number and the properties of stellar streams are likely to be rather different from pure dark-matter streams, it is worth noting that these results are qualitatively similar to

those found for our stellar samples. To try to quantify the degree of similarity, it is simplest to assume that 10% of the particles in these volumes represent stars (i.e. reflecting a “universal” baryon fraction). In this way we can randomly define “stellar samples” which we subject to statistical analysis, such as the velocity correlation function. Such analysis show a weak signal at the 1σ level, which has a smaller amplitude than found for the selected stellar sample discussed in Sect. 3. This result could suggest that stars are not just a random subset of dark-matter particles. This would not be very surprising since stars are expected to be much more clustered in the centers of dark-matter halos.

In principle it should be possible to identify which particles might represent stars using better motivated physical arguments (e.g., by selecting those that have the largest binding energies at redshift ~ 10 , Moore 2001). However, this is not straightforward, as it involves, for example determining the efficiency of star formation in each progenitor halo (Robertson et al. 2005).

In any case, our main limitation in quantifying the degree of similarity between the stellar sample and the dark-matter simulation lies in the number of particles available in this simulation. We expect that typically, only 1 in 250 particles will be a star (Helmi et al. 2003)¹. If this is the case, to reproduce our selected sample with ~ 400 stars our simulations should have 10^5 particles in each volume.

5. Adiabatic invariants

We are also interested in understanding the properties of our selected sample in the space of adiabatic invariants, since this is generally the preferred space to look for evidence of substructures related to past mergers. Here clumping should be strong, since all stars originating from the same progenitor have very similar integrals of motion, resulting in the superposition of the corresponding streams. In particular, Helmi et al. (1999) and Chiba & Beers (2000) have examined the kinematics of metal-poor stars in the solar neighborhood and identified a statistically significant clumping of stars in the angular momentum diagram L_z versus $L_{xy} = \sqrt{L_x^2 + L_y^2}$.

The substructure identified by Helmi et al. (1999) consists of 7 (12) stars with $[\text{Fe}/\text{H}] \leq -1.6$ (-1.0) dex and $D < 1$ (2.5) kpc, and was discovered in a sample that was primarily the result of the combination of HIPPARCOS data with the Beers & Sommer-Larsen catalog (1995). Chiba & Beers, using the Beers et al. (2000) catalog (i.e. a revised edition of the

¹ This is essentially determined by the ratio of mass in dark-matter to that in halo stars for the Solar neighborhood.

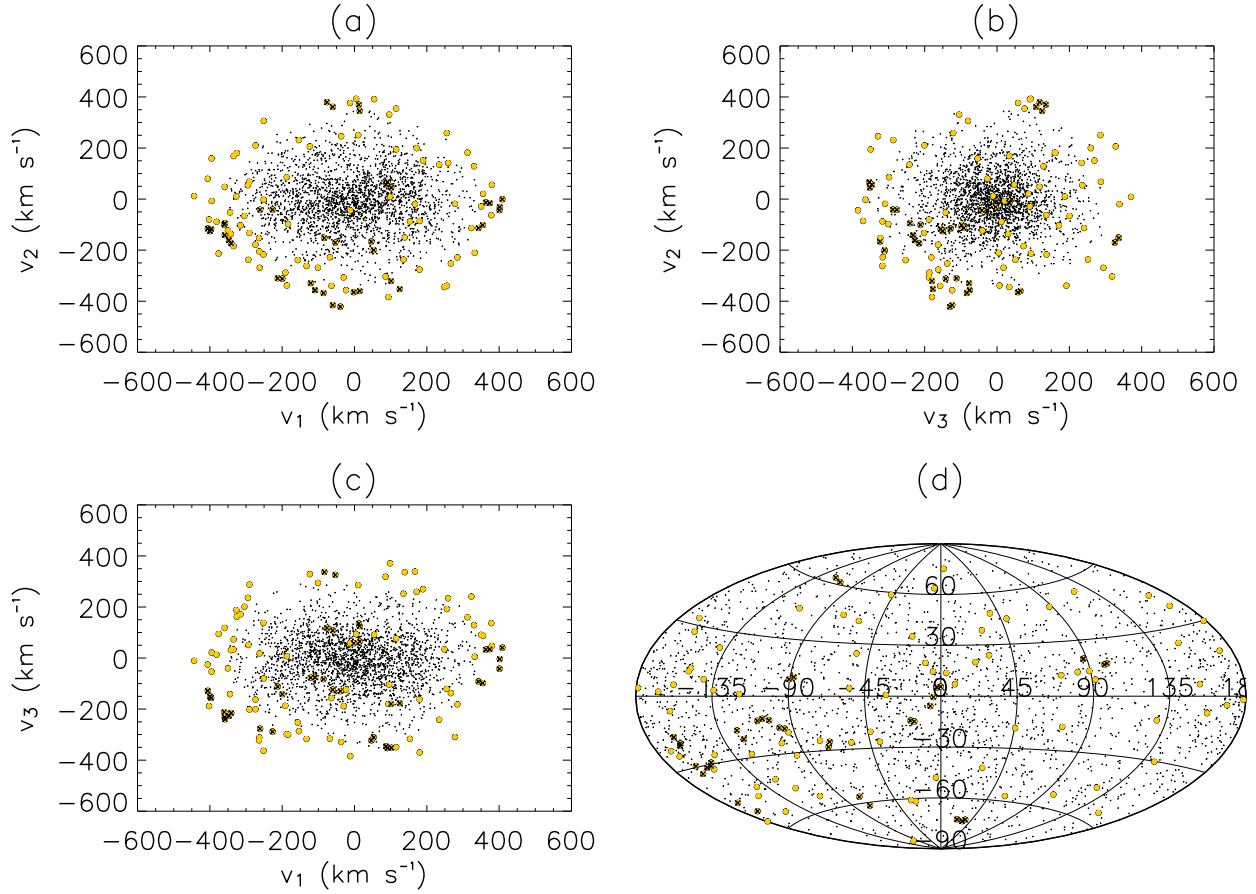


Fig. 4. Distribution of 2348 dark matter particles from a CDM simulation located in a sphere of 2 kpc radius centered at 8 kpc from the Galaxy center. (a-c) Velocity projections in the (v_1, v_2, v_3) space; (d) Velocity directions. The solid gray circles denote the 5% most energetic particles, while the asterisks identify those subsets whose velocity difference is less than 42 km s^{-1} . The kinematics characteristics observed in this set of plots are representative of what is seen in other similar volumes.

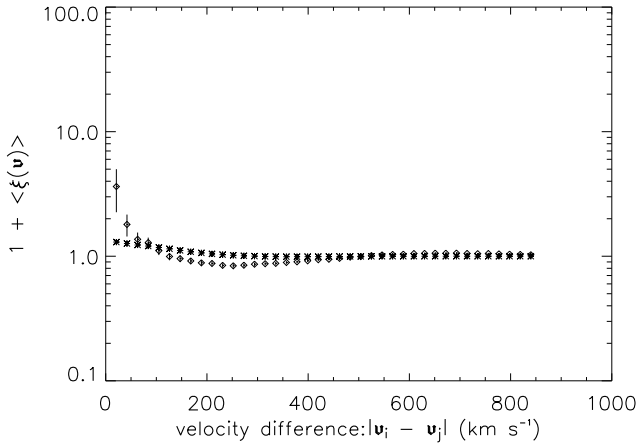


Fig. 5. Velocity correlation function $\xi(v)$ for the volume shown in Fig. 4. Asterisks and diamonds correspond to ξ for the full sample and for the subset of 5% fastest moving particles, respectively.

previous compilation) confirmed 9 of their stars in the clump region which includes also one of the stars in our kinematic group, HD214161. However, they later discarded this star for having quite different orbital properties than other clump members.

Here we focus on the space of adiabatic invariants E , L_z and L_{xy} , although the latter is not fully conserved in an axisymmetric potential, and its use may not be generally appropriate for the study of substructure in the halo. Nevertheless, we hope to obtain further insight into our previous analysis based only on kinematics. We assume that the Galactic potential is represented by three components (Johnston et al. 1996): a dark halo with logarithmic potential, a Miyamoto-Nagai disk, and a spherical Hernquist bulge:

$$\begin{aligned} \Phi_{\text{halo}} &= v_h^2 \ln \frac{r^2 + d^2}{r_{200}^2} \\ \Phi_{\text{disk}} &= -\frac{GM_{\text{disk}}}{\sqrt{R^2 + (a + \sqrt{z^2 + b^2})^2}} \\ \Phi_{\text{bulge}} &= -\frac{GM_{\text{bulge}}}{r+c} \end{aligned} \quad (4)$$

where $M_{\text{disk}} = 1.0 \times 10^{11} M_{\odot}$, $M_{\text{bulge}} = 3.4 \times 10^{10} M_{\odot}$; $v_h = 131.5 \text{ km s}^{-1}$ and $r_{200} = 300 \text{ kpc}$; $a = 6.5 \text{ kpc}$, $b = 0.26 \text{ kpc}$,

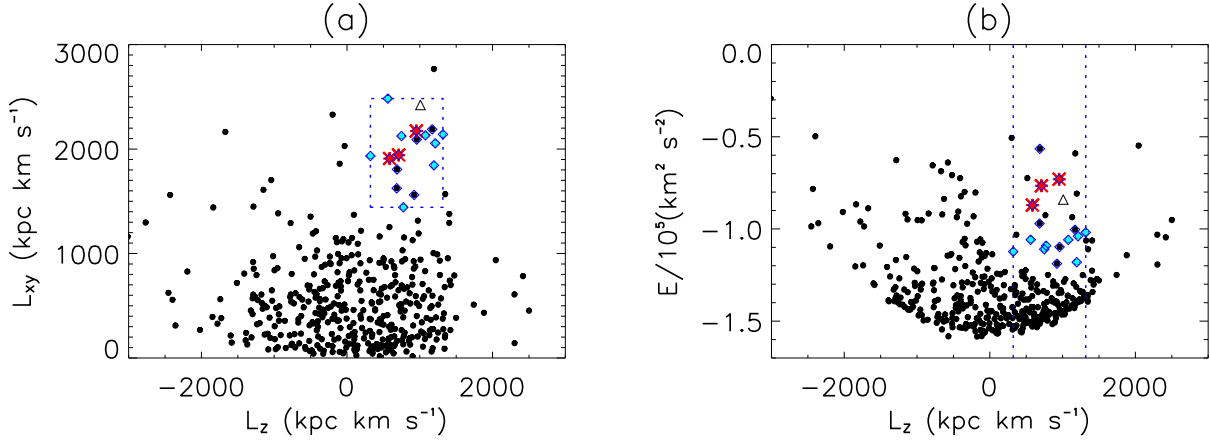


Fig. 6. Distribution of the selected sample of 410 stars with $D < 2$ kpc in the space of adiabatic invariants. The asterisks denote our kinematic group (RHLS), and the grey diamonds the clump identified by Helmi et al. (1999) (HWdZZ). These stars are used to define a region (limited by the dashed lines in the left panel), which encompasses also other stars with similar angular momenta, and which are indicated as diamonds in both panels. CD – 80 328, the candidate from the Nordström et al. (2004) catalog, has been added and is shown as a triangle.

$c = 0.7$ kpc, and $d = 12$ kpc. This choice of parameters gives a circular velocity at the solar radius of 210 km s^{-1} .

Figure 6 shows the distribution of the selected sample within 2 kpc of the Sun, in the space of adiabatic invariants. Note that the sample includes 8 stars (hereafter HWdZZ stars) from the stream identified by Helmi et al. (1999). These stars are shown by gray solid diamonds while our kinematic clump (hereafter RHLS) is plotted as asterisks. It is clear that these groups have similar momenta (see left panel). If L_{xy}^{\min} (L_z^{\min}) and L_{xy}^{\max} (L_z^{\max}) denote the minimum and maximum L_{xy} (L_z) values for the HWdZZ and RHLS stars, the region $L_{xy}^{\min} < L_{xy} < L_{xy}^{\max}$ and $L_z^{\min} < L_z < L_z^{\max}$ (dotted box) encompasses stars with similar momenta. There are 16 stars located in this region, which include five new objects shown as black diamonds in Fig. 6. Some of these stars are also members of the ‘clump-trail’ structure identified by Chiba & Beers (2000) (hereafter CB). The orbital properties of these 16 stars, based on the Galactic potential defined above, are listed in Table 3. The last column serves to indicate the membership to the various groups.

We have looked for additional members of our kinematic group in the Nordström et al. (2004) catalog of nearby stars. Selecting stars with $[\text{Fe}/\text{H}] \leq -1.5$ dex and similar kinematic characteristics as those we identified, we find only one possible candidate. CD – 80 328 is a metal poor star ($[\text{Fe}/\text{H}] = -1.98$ dex) with $(U, V + 220, W) = (-193, 125, 303) \text{ km s}^{-1}$ and a highly eccentric orbit $e = 0.83$. It is shown as a triangle in Fig. 6. CD – 80 328, having $L_z = 1009 \text{ kpc km s}^{-1}$ and $L_{xy} = 2422 \text{ kpc km s}^{-1}$, is located well within the box-region defined by the HWdZZ stars. However, given its much lower binding energy ($E = -0.84 \cdot 10^5 \text{ km}^2 \text{ s}^{-2}$), it is more likely that CD – 80 328 is a member of our moving group.

According to numerical simulations carried out by Brook et al. (2003), stars from an accreted satellite show typically highly eccentric orbits ($e > 0.8$) and strongly correlated velocities. In view of this, the stars of our kinematic group

(with $0.81 < e < 0.85$) could well share a common origin, and be stellar debris from an accreted satellite.

It is worth noting that, while having similar momenta, our kinematic structure and the HWdZZ clump have somewhat different energies. This could imply that these groups have different origin. However, it seems also plausible that these groups have been stripped off from the *same* progenitor at different times. In this scenario, HWdZZ stars should have been released in a later galactic passage than those in our kinematic clump. The difference in orbital energy between the groups could be the result of different binding energies of the progenitor galaxy (higher and lower, respectively) due to the effects of dynamical friction upon this system while orbiting the Milky Way.

6. Conclusions

We have extracted samples of metal-poor ($[\text{Fe}/\text{H}] \leq -1.5$ dex) halo stars in the Solar neighborhood from Beers et al. (2000) catalog, and carried out a statistical analysis of their kinematics.

Based on clustering in the velocity space, we have found evidence of substructures in the motions of the fastest moving stars, at a level which seems to be consistent with that predicted by high resolution simulations of dark matter halos in a hierarchical universe.

The moving group responsible for this signal is comprised by three stars, whose kinematic and metallicity characteristics are similar to the streams found by Helmi et al. (1999), albeit on somewhat more loosely bound orbits.

Our sample of halo and high velocity stars is too small to make definite statements about the importance of accretion in the formation of the Galactic halo. This would require a sample with a few thousands nearby halo stars (i.e., ~ 10 times larger than our selected sample) with accurate space velocities. Such sample sizes will become available in the near future, thanks to spectroscopic surveys like RAVE (Steinmetz 2003)

Table 3. Characteristics of the stars located in the region $L_{xy}^{\min} < L_{xy} < L_{xy}^{\max}$ and $L_z^{\min} < L_z < L_z^{\max}$ defined by the Helmi et al. (1999) structure (within the box shown in the left panel of Fig. 6.)

Name	[Fe/H] (dex)	$E/10^5$ ($\text{km}^2 \text{s}^{-2}$)	L_z (kpc km s^{-1})	L_{xy} (kpc km s^{-1})	e	Membership
BPS CS 22948-0093	-3.72	-0.57	687	1805	0.92	
HD 214161	-2.16	-0.73	952	2173	0.81	RHLS
V* RZ Cep	-1.77	-0.77	710	1943	0.85	RHLS
BPS CS 30339-0037	-2.13	-0.87	586	1909	0.81	RHLS
BPS CS 22189-0007	-2.12	-0.97	683	1624	0.77	
BPS CS 29513-0031	-2.79	-1.00	1171	2189	0.47	CB
BD+10 2495	-1.83	-1.02	1318	2140	0.47	HWdZZ, CB
HD 119516	-2.49	-1.04	1212	2055	0.50	HWdZZ, CB
V* TT Cnc	-1.57	-1.06	562	2483	0.42	HWdZZ
CD-36 1052	-2.19	-1.06	1078	2132	0.45	HWdZZ, CB
HD 237846	-2.63	-1.09	774	1443	0.71	HWdZZ
BPS CS 29504-0044	-2.04	-1.10	958	2091	0.42	CB
V* AR Ser	-1.78	-1.12	322	1934	0.46	HWdZZ
V* TT Lyn	-1.56	-1.11	748	2124	0.45	HWdZZ, CB
HD 128279	-2.20	-1.18	1194	1844	0.23	HWdZZ, CB
BPS CS 22876-0040	-2.20	-1.19	922	1561	0.42	CB

Membership: RHLS: Re Fiorentin et al. (this paper); HWdZZ: Helmi et al. (1999); CB: Chiba & Beers (2000)

and SDSS-II/SEGUE (Beers et al. 2004), which could be combined with proper motion catalogs such as UCAC2 (Zacharias et al. 2004), SPM (Platais et al. 1998), GSC-II (McLean et al. 2000), USNO-B (Monet et al. 2003), to obtain full phase-space information.

The existence of structures in the halo, if confirmed by further studies, is of great importance for constraining models of the formation and evolution of the Galaxy. The space astrometric mission Gaia (Perryman et al. 2001) will collect samples of millions of stars in our Galaxy as well as in our nearest neighbours with very accurate positions, proper motions, and trigonometric parallaxes which will dramatically improve the situation, and revolutionize our knowledge of the Galaxy.

Acknowledgements. We wish to thank Volker Springel and Simon White who allowed us to use data from their simulations; Antonaldo Diaferio and Ronald Drimmel for suggestions and many useful comments; Attilio Ferrari for his constant support to this project. This work was initiated at the Astronomical Institute in Utrecht, which is gratefully acknowledged. P.R.F. wishes to thank the Astronomical Institute in Utrecht for hospitality during her visit. Partial financial support to this research comes from the Italian Ministry of Research (MIUR) through the COFIN-2001 program, and from the Netherlands Organization for Scientific Research (NWO) and the Netherlands Research School for Astronomy (NOVA). Finally, we thank the referee, Timothy Beers, for a careful reading of this manuscript and for his useful remarks.

References

Beers, T.C., & Sommer-Larsen, J. 1995, *ApJ*, 96, 175
 Beers, T.C., Chiba, M., Yoshii, Y., et al. 2000, *ApJ*, 119, 2866

Beers, T.C., Allende P.C., Wilhelm, R., et al. 2004, *PASA*, 21, 207
 Binney, J., & Merrifield, M. 1998, *Galactic Astronomy*. (Princeton: Princeton Univ. Press)
 Brook, C.B., Kawata, D., Gibson, B. K., & Flynn, C. 2003, *ApJ*, 585, L125
 Chiba, M., & Beers, T.C. 2000, *AJ*, 119, 2843 (CB)
 Chiba, M., & Beers, T.C. 2001, *ApJ*, 549, 325
 Coil, A.L., Newman, J.A., Kaiser, N., et al. 2004, *ApJ*, 617, 765
 Dehnen, W., & Binney, J.J. 1998, *MNRAS*, 298, 387
 Diemand, J., Moore, B., & Stadel, J. 2005, *Nature*, 433, 389
 Eggen, O.J., Lynden-Bell, D.A., & Sandage, A.R. 1962, *ApJ*, 136, 748
 Ferguson, A.M.N., Irwin, M.J., Ibata, R.A., et al. 2002, *AJ*, 124, 1452
 Helmi, A., White, S.D.M., de Zeeuw, P.T., & Zhao, H.S. 1999, *Nature*, 402, 53 (HWdZZ)
 Helmi, A., White, S.D.M., & Springel, V. 2002, *Phys. Rev. D*, 66, 063502
 Helmi, A., White, S.D.M., & Springel, V. 2003, *MNRAS*, 339, 834
 Helmi, A. 2004a, *MNRAS*, 351, 643
 Helmi, A. 2004b, *ApJ*, 610, L97
 Ibata, R.A., Gilmore, G., & Irwin, M.J. 1995, *MNRAS*, 277, 781
 Johnston, K.V., Hernquist, L., & Bolte, M. 1996, *ApJ*, 465, 278
 Kerscher, M., Szapudi, I., & Szalay, A.S. 2000, *ApJ*, 535, L13
 Law, D.R., Johnston, K.V., & Majewski, S.R. 2005, *ApJ*, 619, 807

- Lemon, D.J., Wyse, R.F.G., Liske, J., Driver, S.P., & Horne, K. 2004, *MNRAS*, 347, 1043
- Majewski, S.R., Munn, J.A., & Hawley, S.L. 1996, *ApJ*, 456, L73
- Martin, N.F., Ibata, R.A., Bellazzini, M., et al. 2004, *MNRAS*, 348, 12
- McLean, B.J., Greene, G.R., Lattanzi, M. G., & Pirenne, B. 2000, *ASPC*, 216, 145
- Monet, D.G., Levine, S.E., Canzian, B., et al. 2003, *AJ*, 125, 984
- Moore, B., Calcanoe-Roldan, C., Stadel, J., et al. 2001, *Phys. Rev. D*, 64, 063508
- Moore, B. 2001, *AIPC*, 586, 73
- Mullis, C.R., Henry, J.P., Gioia, I.M., et al. 2004, *ApJ*, 617, 192
- Newberg, H.J., Yanny, B., Rockosi, C., et al. 2002, *ApJ*, 569, 245
- Nordström, B., Mayor, M., Andersen, J., et al. 2004, *A&A*, 418, 989
- Perryman, M.A.C., de Boer, K.S., Gilmore, G., et al. 2001, *A&A*, 369, 339
- Platais, I., Girard, T.M., Kozhurina-Platais, V., et al. 1998, *AJ*, 116, 2564
- Reid, I.N., & Majewski S.R. 1993, *ApJ*, 409, 635
- Robertson, B., Bullock, J.S., Font, A.S., Johnston, K.V., & Hernquist, L. 2005, *astro-ph/0501398*
- Robin, A.C., Haywood, H., Crézé, M., Ojha, D. K., & Bienaymé, O. 1996, *A&A*, 305, 125
- Searle, L., & Zinn, R. 1978, *ApJ*, 225, 357
- Springel, V., White, S.D.M., Tormen, G., & Kauffmann, G. 2001, *MNRAS*, 328, 726
- Steinmetz, M. 2003, *ASPC*, 298, 381
- Zacharias, N., Urban, S.E., Zacharias, M.I., et al. 2004, *A&A*, 417, 3043
- Zheng, Z., Shang, Z., Su, H., et al. 1999, *AJ*, 117, 2757
- Zhao, H., Taylor, J.E., Silk, J., & Hooper, D. 2005, *astro-ph/0502049*